Ultrafast Electron Transfer and Coupled Vibrational Dynamics in Cyanide Bridged Mixed-Valence Transition-Metal Dimers

Stephen K. Doorn,† R. Brian Dyer,‡ Page O. Stoutland,*,‡ and William H. Woodruff†

Contribution from the Divisions of Chemistry and Laser Sciences (Mail Stop J-567) and Isotope and Nuclear Chemistry (Mail Stop C-345), Los Alamos National Laboratory, Los Alamos, New Mexico 87545

Received December 18, 1992

Abstract: Picosecond infrared spectroscopy has been used to investigate electron transfer and vibrational excitation and relaxation in the mixed-valence transition-metal dimer $[(NC)_5M^{II}CNM^{III}(NH_3)_5]^-$ (M = Ru, Os). Optical excitation into the metal-to-metal charge transfer band results in formation of the excited state redox isomer $[(NC)_5M^{III}CNM^{II}(NH_3)_5]^-$. Subsequent back electron transfer results in reformation of the ground state and occurs with $\tau < 0.5$ ps. Upon return to the ground electronic state, large amounts of energy (up to 7 quanta, 14 000 cm^{-1}) are placed into the terminal MC≡N stretching mode. The rate of the subsequent energy relaxation was measured; decay times ranged from <0.5 to 6 ps for the ruthenium analog and from 1.8 to 18 ps for the osmium analog. Results are compared to recent theoretical models of Jortner and Bixon.

Introduction

Ultrafast electron transfer reactions are at the heart of important fundamental processes including the initial charge separation occurring in photosynthetic reaction centers.[1] Understanding the microscopic details of these reactions has been the object of much recent work, and is central to, for example, the design of efficient synthetic solar energy conversion materials. In addition, the details of ultrafast electron transfer reactions have direct implications for the development of molecular level devices such as ultrafast optical switches, conducting polymer films, and molecular wires.[2] Recent studies in the area of ultrafast electron transfer have centered on understanding the factors which govern the rates of these reactions. Specifically, in addition to considering how thermodynamics affect the rates of electron transfer reactions, recent experimental[3] and theoretical[4] work has shown the importance of considering the dynamical role of the solvent, and of coupled intramolecular vibrations. For example, ultrafast electron transfer rates have often been found to correspond to the dielectric relaxation time of the solvent, suggesting that in the absence of other limiting factors (i.e. thermodynamic barriers), rates of electron transfer reactions are limited by what has been termed the "dielectric friction" of the solvent.[3b] In some cases, however, electron transfer rates have been observed to greatly exceed the dielectric relaxation time of the solvent; calculations have suggested that high-frequency ($h\nu >> kT$) intramolecular modes coupled to the electron transfer are responsible for this rate acceleration.[4c] Thus, in addition to considering the dynamical effects of the solvent, it has become increasingly apparent that, in some cases, it is also necessary to consider nuclear motions associated with intramolecular vibrational modes.

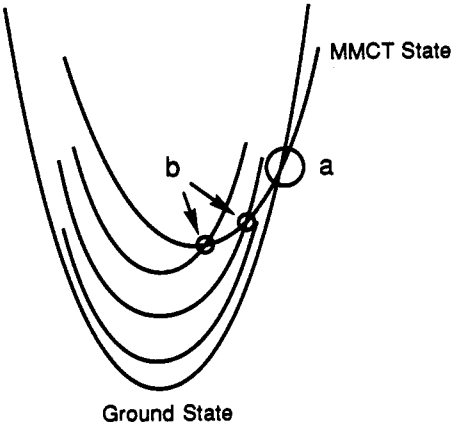

Figure 1. Potential energy diagram for the electron transfer process showing the reaction along the solvent coordinate. Inclusion of a high-frequency quantal vibration (i.e. vibrations orthogonal to the solvent coordinate) lowers the potential energy barrier (points b) to the back electron transfer reaction in comparison to the classical barrier crossing at point a.

Recent models[5] have sought to quantify the dynamical effects of high-frequency intramolecular vibrations that have been shown to be especially important for electron transfer reactions occurring in the "Marcus inverted region". In the classical view of these cases, electron transfer can occur only at curve crossings (Figure 1). Inclusion of high-frequency quantal modes, however, accelerates the electron transfer by providing additional, lower energy, curve crossings. Importantly, these models suggest that not only should high-frequency modes accelerate the rate of electron transfer, but that the products should have high degrees of vibrational excitation in the coupled intramolecular vibrational modes. There have, however, been no direct experimental tests of this prediction.

We have recently been interested in a class of compounds known as mixed-valence transition-metal dimers which provide a well-

* Author to whom correspondance should be addressed.
† Isotope and Nuclear Chemistry.
‡ Chemistry and Laser Sciences.

(1) See, for example: (a) *Photosynthesis*; Stachlin, L. A., Arntzen, C. J., Ed.; Springer-Verlag: New York, 1986; Vol. 1, p 3. (b) *Photosynthesis*; Govindje, Ed.; Academic Press: New York, 1982; Vol. 1. (c) Danks, S. M.; Evans, E. H.; Whittaker, P. A. *Photosynthetic Systems*; Wiley: New York, 1983. (d) Sauer, K. *Annu. Rev. Phys. Chem.* **1979**, *30*, 155.

(2) *Molecular Electronic Devices*, Carter, F. L., Ed.; Marcel Dekker, Inc.: New York, 1982.

(3) For recent reviews, see: (a) Simon, J. D. *Acc. Chem. Res.* **1988**, *21*, 128. (b) Barbara, P. F.; Jarzeba, W. *Adv. Photochem.* **1990**, *15*, 1. See, also: (c) Walker, G. C.; Aakesson, E.; Johnson, A. E.; Levinger, N. E.; Barbara, P. F. *J. Phys. Chem.* **1992**, *96*, 3728. (d) Barbara, P. F.; Walker, G. C.; Smith, T. P. *Science* **1992**, *256*, 975 and references therein.

(4) (a) Sumi, H.; Marcus, R. A. *J. Chem. Phys.* **1986**, *84*, 4894. (b) Rips, I.; Jortner, J. *J. Chem. Phys.* **1987**, *87*, 2090. (c) Jortner, J.; Bixon, M. *J. Chem. Phys.* **1987**, *88*, 167. (d) Newton, M. D.; Sutin, N. *Annu. Rev. Phys. Chem.* **1984**, *35*, 437. (e) Bixon, M.; Jortner, J. *J. Phys. Chem.* **1991**, *95*, 1941. (e) Weaver, M. J.; McManis, G. E., III *Acc. Chem. Res.* **1990**, *23*, 294.

(5) For a review of progress in this area, see: Newton, M. D.; Sutin, N. *Annu. Rev. Phys. Chem.* **1985**, *35*, 437 and ref 3d.

0002-7863/93/1515-6398$04.00/0

defined environment in which to study electron transfer reactions.[6] Specifically, we have used picosecond infrared spectroscopy to investigate a number of cyanide-bridged mixed-valence dimers of the form:

$$[(CN)_5M^{II}\text{–}CN\text{–}M^{III}(NH_3)_5]^-$$

Mixed-valence dimers have historically been attractive model systems for studies of electron transfer.[7] This attraction arises from the presence of two well-defined metal sites of differing oxidation state in which there is the possibility of observing an inner-sphere electron transfer between the two metal centers. Optical excitation into the metal-to-metal charge transfer (MMCT) band leads to formation of the excited state redox isomer:

$$[(NC)_5Ru^{II}CNRu^{III}(NH_3)_5]^- \overset{h\nu}{\underset{ET}{\rightleftharpoons}} [(NC)_5Ru^{III}CNRu^{II}(NH_3)_5]^-$$

Subsequent thermal back electron transfer results in reformation of the original species. Simple models originally developed by Hush[8] have linked the energy of the optical charge transfer to the barrier for the thermal back electron transfer. Despite the simplicity of these models, they have been shown to be consistent with the available experimental evidence, and thus have proven to be valuable tools in understanding electron transfer reactions. For example, simple static optical absorption experiments[9] have yielded information on such aspects of electron transfer as the electronic coupling between donor and acceptor, solvation effects on band energies and coupling, and the magnitude of the activation barriers to the thermal electron transfer. While these studies have been instrumental in testing and modifying various aspects of electron transfer theories, direct tests of electron transfer barrier (and thus the rate) predictions have been difficult, in part because MMCT bands are typically located in the near-infrared region of the spectrum and have very low oscillator strengths.

The absorption characteristics of the cyanide-bridged dimers, however, make them more suitable for kinetic studies from which the electron transfer barrier might be directly extracted. Because of the large differences in redox potentials between the two metal centers (about 0.9 eV for Ru–Ru and 1.2 eV for Os–Os[10]) the MMCT band is in the visible region of the spectrum and is isolated from other optical transitions. This feature made possible the recent measurements of the electron transfer dynamics by Barbara et al.[11] of the Ru–Fe and the Ru–Ru derivatives using femtosecond visible absorption spectroscopy. Furthermore, the accessibility of lasers in the visible region of the spectrum has also made it possible to obtain resonance Raman spectra of these molecules.[12] Resonance Raman investigations in which the probe laser is resonant with the charge transfer band provide direct, detailed information on the vibrational modes coupled to the electron transfer reaction.

Our measurements are complementary to these in that picosecond infrared spectroscopy provides, within one experiment, the possibility of observing both the dynamics of the electron transfer and vibrational excitation/relaxation of the modes coupled to the transition. For example, the frequencies of MC≡N stretching vibrations are very sensitive to the formal charge at the metal center and, because of anharmonicity, to the degree of excitation in a particular mode. Historically, there have been questions concerning the extent of localization of the excess electron in mixed-valence systems (i.e. Is the system best described as $M^{2.5+}$–$M^{2.5+}$ or M^{3+}–M^{2+}?). In the cyanide-bridged dimer described here, strong asymmetry in the molecule leads to a localized ground state despite the strong coupling between the two metal centers, but it is conceivable that in the electronically excited state the excess electron might be delocalized. The experiments described here are thus able to address questions concerning the rate of electron transfer, the extent of charge transfer, and the role of coupled intramolecular vibrations.

Experimental Section

Experiments were performed using visible pump pulses and infrared probe pulses where time resolution is obtained by spatially delaying the probe pulse relative to the pump pulse (Figure 2).[13] Picosecond pulses originate in a dual-jet dye laser synchronously pumped at 76 MHz by the frequency-doubled output of a cw mode-locked Nd:YAG laser (Coherent Antares 76-S). Operating on Rhodamine 6G/DODCI, the dye laser (homebuilt) provides pulses of ca. 2 ps (fwhm = 8 cm^{-1}, pulse energies ~ 1 nJ/pulse) tunable using a two-plate birefringent filter throughout the gain curve of the dye (ca. 580-640 nm). Useful pulse energies are obtained by passing the dye laser output through a three-stage dye amplifier (Kiton Red 620) pumped at 30 Hz by the frequency-doubled output (ca. 15 mJ/pulse at 532 nm) of a regeneratively amplified Nd:YAG laser (Continuum RGA-60-30). Amplification increases the pulse energy to ~200 μJ/pulse with minimal pulse broadening.

The pump (or excitation) pulse is either the amplified dye laser pulse itself (typically attenuated to 30 μJ/pulse) or is formed using the technique of continuum amplification. In this case, the amplified dye laser pulse is focused into a 2-cm cuvet of H_2O to form a white light continuum. This is then collimated and sent through a filter to select the desired wavelength. Subsequent amplification in two stages results in 2-ps pulses of ~100 μJ/pulse. For the experiments described here, the 700-nm pump pulse was obtained by passing the continuum through a 10 nm fwhm interference filter centered at 700 nm and subsequently amplifying it in LDS 698 to 50–100 μJ/pulse (later attenuated to 30 μJ/pulse).[14]

Infrared probe pulses in the 5-μm region are generated in a 5 mm thick $LiIO_3$ crystal by difference frequency mixing the visible dye laser pulse (~10 μJ/pulse) with the 532-nm pulses (75 ps, ~100 μJ/pulse) from the regeneratively amplified Nd:YAG laser. The resultant IR pulses are ~2 ps fwhm, 10–100 nJ/pulse, with a frequency bandwidth of ca. 8 cm^{-1}. Tuning of the infrared probe pulse is accomplished by changing the output wavelength of the dye laser. Using the present dye/crystal combination, the infrared probe can be tuned between 2900 and 1800 cm^{-1} which corresponds to changing the dye laser wavelength from 629 to 588 nm.

The infrared pulses are split into reference and sample beams and are detected by matched indium:antimonide (InSb) detectors. Subsequently, the detector signals are integrated (Stanford SR250), ratioed (Stanford SR235), and transferred to a Macintosh IIx computer for further data analysis. The visible pump beam is blocked at 15 Hz with a shutter to yield light on/light off data, allowing the determination of absolute ΔA's

(6) Preliminary reports of our work have been published: (a) Doorn, S. K.; Stoutland, P. O.; Dyer, R. B.; Woodruff, W. H. *J. Am. Chem. Soc.* **1992**, *114*, 3133. (b) Stoutland, P. O.; Dyer, R. B.; Woodruff, W. H. *Science* **1992**, *257*, 1913.

(7) See, for example: (a) *Mixed-Valence Compounds*; Brown, D. B., Ed.; D. Reidel: Dordrecht, The Netherlands, 1980. (b) Creutz, C. *Prog. Inorg. Chem.* **1983**, *30*, 1.

(8) (a) Hush, N. S. *Prog. Inorg. Chem.* **1967**, *8*, 391. (b) Hush, N. S. *Electrochim. Acta* **1968**, *13*, 1005. (c) Hopfield, J. J. *Proc. Natl. Acad. Sci. U.S.A.* **1974**, *21*, 3640. (d) Hopfield, J. J. *Biophys. J.* **1977**, *18*, 311. (e) Potasek, M. J.; Hopfield, J. J. *Proc. Natl. Acad. Sci. U.S.A.* **1977**, *74*, 229, 3817. (f) Meyer, T. J. *Prog. Inorg. Chem.* **1983**, *30*, 389.

(9) (a) Itskovitch, E. M.; Ulstrup, J.; Vorotyntsev, M. A. In *The Chemical Physics of Solvation*; Dogonadze, R. R., Kalman, E., Kornyshev, A. A., Ulstrup, J., Eds.; Elsevier: Amsterdam, 1986; Part B. (b) Blackbourn, R. L.; Doorn, S. K.; Roberts, J. A.; Hupp, J. T. *Langmuir* **1989**, *5*, 696 and references therein.

(10) Estimated from redox potentials for the appropriate monomer pairs, see: Haim, A. *Inorg. Chem.* **1985**, *14*, 113.

(11) (a) Walker, G. C.; Barbara, P. F.; Doorn, S. K.; Dong, Y.; Hupp, J. T. *J. Phys. Chem.* **1991**, *95*, 5712. (b) Kliner, D. A. V.; Tominaga, K.; Walker, G. C.; Barbara, P. F. *J. Am. Chem. Soc.* **1992**, *114*, 8323.

(12) (a) Doorn, S. K.; Hupp, J. T. *J. Am. Chem. Soc.* **1989**, *111*, 1142. (b) Doorn, S. K.; Blackbourn, R. L.; Johnson, C. S.; Hupp, J. T. *Electrochim. Acta* **1991**, *36*, 1775. (c) Doorn, S. K. Ph.D. Dissertation, Northwestern University, 1990.

(13) For a recent review of the technological aspects of ultrafast infrared spectroscopy, see ref 6b.

(14) When performing experiments using a pump pulse formed by amplifying part of a white light continuum, larger "coherence artifacts" were observed. We believe this occurs because the pulse is actually highly structured (temporally) due to the process of continuum formation. Thus while the *average* pulse shape is well-described by a $sech^2$ function, a single pulse would be more accurately described as a highly structured pulse composed of many subpicosecond features. Such structure would tend to accentuate "coherence artifacts".

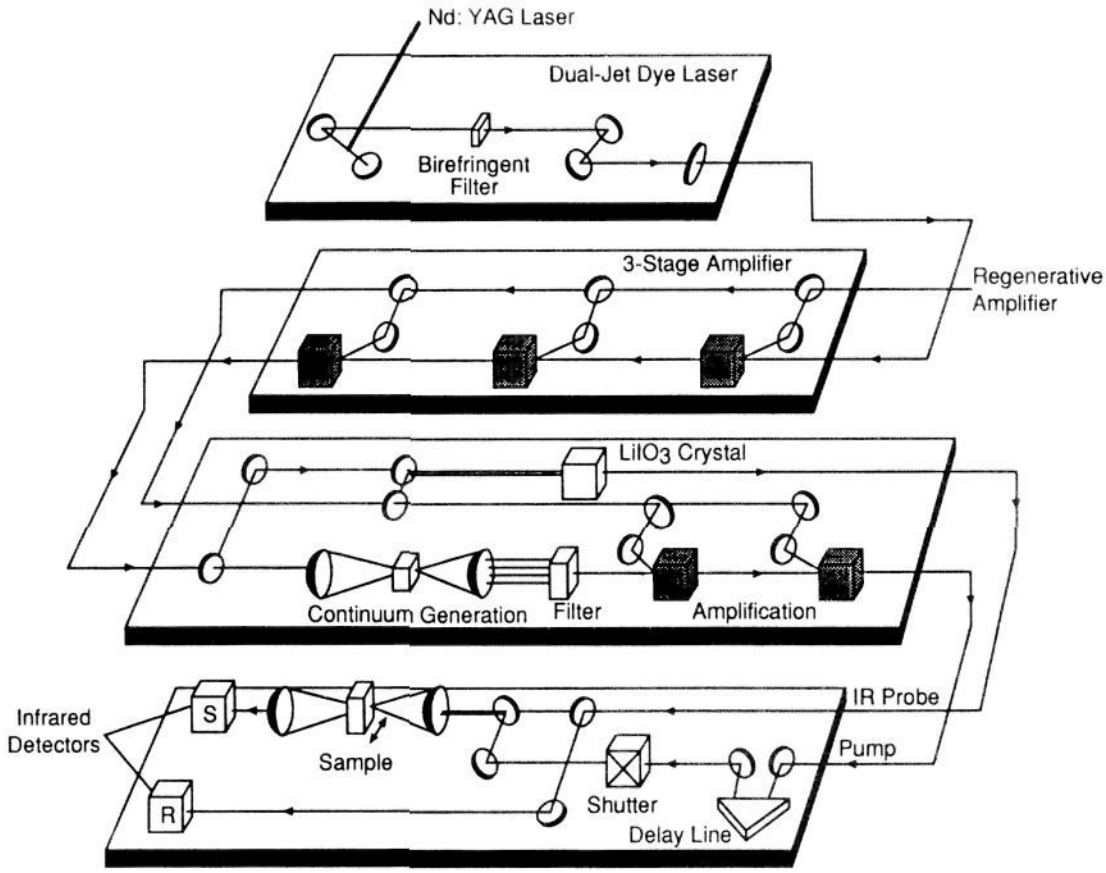

Figure 2. Schematic of the picosecond time resolved infrared apparatus.

and improving the S/N ratio by 3–4 times.[15] Typical transients are averages of 4 to 10 scans, with 50 samples being collected at each delay time for each individual scan. Our apparatus as described is capable of detecting absorbance changes of ~0.1%.

The instrument response function and the zero of time are determined by substituting a wafer of silicon in place of the sample.[16] Excitation by the pump pulse results in a subpicosecond decrease in transmission throughout the infrared, thus decreasing the observed probe intensity as the two pulses are overlapped in time. Typical pump-probe cross-correlations are 3–4 ps fwhm and are well described by a sech^2 function. Using deconvolution techniques on transients with typical signal to noise, we can resolve events with rise/decay times of ~0.5 ps.

The mixed-valence dimers were prepared according to literature methods.[17] Typical samples are 0.04 M solutions of dimer in D_2O or twice the concentration in H_2O. Solutions are loaded into 100 or 50 μm (for D_2O and H_2O, respectively) pathlength IR cells fitted with CaF_2 windows. The ground state visible spectra of the Ru–Ru and Os–Os dimers are shown in Figure 3. The MMCT bands are centered at 683 (ϵ = 2800 M^{-1} cm^{-1}) and 560 nm (ϵ = 2100 M^{-1} cm^{-1}), respectively. The structure observed in the Os–Os spectrum is due to partial resolution of splitting of the charge transfer transition due to spin–orbit coupling. The ground state infrared spectrum of the Ru–Ru dimer is shown in Figure 4. We observe one strong band at 2053 cm^{-1} (fwhm = 23 cm^{-1}, ϵ = 2500 M^{-1} cm^{-1}) corresponding to the terminal RuC≡N stretching mode.[18] We do observe a band attributable to the bridging cyanide at 2118 cm^{-1}, but it is ca. 50 times weaker than the terminal stretching mode. The spectrum for the Os–Os dimer is similar, with the terminal stretching mode occurring at 2040 cm^{-1}.

(15) While we are unsure as to why this improves our S/N ratio, we assume it is because it diminishes the effect of low-frequency noise.

(16) Yen, R.; Shank, C. V.; Hirlimann, C. *Mater. Res. Soc. Symp. Proc.* **1983**, *13*, 13.

(17) (a) Vogler, A.; Kisslinger, J. *J. Am. Chem. Soc.* **1982**, *104*, 2311. (b) Vogler, A.; Osman, A. H.; Kunkely, H. *Inorg. Chem.* **1987**, *26*, 2337.

(18) In C_{4v} symmetry there should be more than one band in this region (excluding the bridging cyanide stretch). Compounds of this type, however, often show only one IR active stretching vibration, perhaps because of their closeness to O_h symmetry.

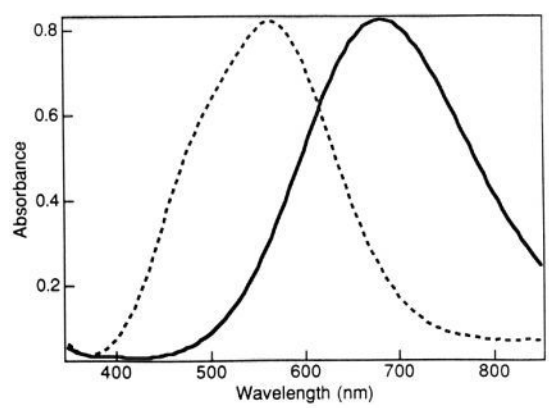

Figure 3. Visible absorption spectra of Ru–Ru (solid line) and Os–Os (dashed line) dimers in H_2O.

Results

In our experiments we excite into the MMCT band of the dimer and probe the subsequent dynamics by monitoring spectral changes in the cyanide stretching region (1900–2200 cm^{-1}) with the infrared probe pulse. Following excitation of the MMCT transition at 600 nm for Ru–Ru in D_2O, we observe an instrument-limited decrease in absorbance of the ground state infrared band followed by a recovery that is best fit by convolving the instrument response with a 6 ± 1 ps exponential (Figure 5a). Probing at higher frequencies reveals a new positive absorbance feature centered at 2110 cm^{-1}, which appears and decays within our instrumental resolution (τ < 0.5 ps, Figure 6). We also observe a new broad absorption at lower energies from the ground state band, appearing between 1950 and 2040 cm^{-1}. Shown in Figure 7 are three kinetic traces taken throughout this region. The rise times of the transients at the low-energy side of this band are

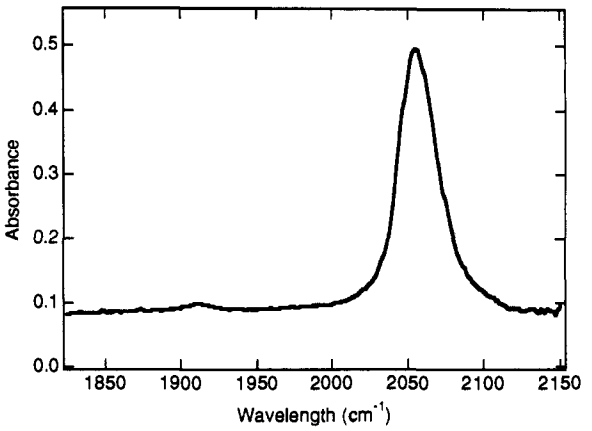

Figure 4. Ground state FTIR spectrum of Ru–Ru in D_2O.

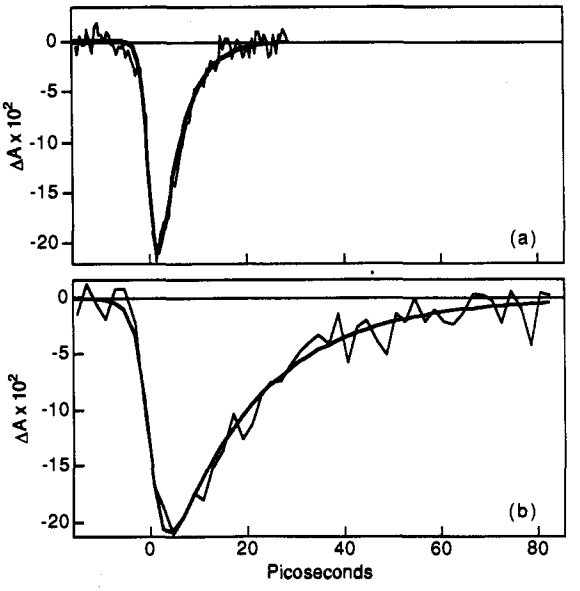

Figure 5. Kinetic traces of the ground state absorbances acquired at (a) 2060 cm^{-1} in Ru–Ru and (b) 2050 cm^{-1} in Os–Os following excitation at 600 nm. Experimental traces are overlayed with calculated best fits to the data.

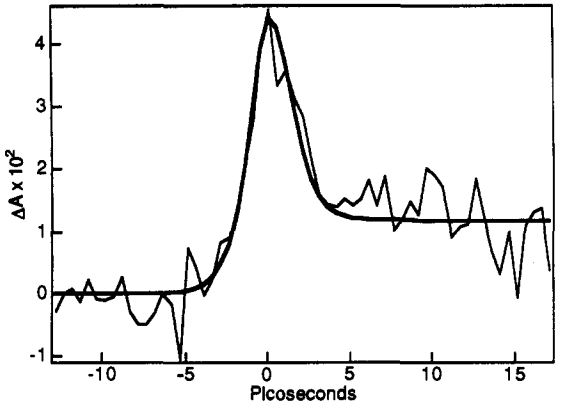

Figure 6. Transient decay obtained at 2110 cm^{-1} from 0.04 M Ru–Ru in D_2O following 600-nm excitation. Offsets remaining at long times (see Figure 7 also) are due to thermal transients and do not affect the fits obtained.

instrumentally limited, but they become progressively slower toward the high energy side of the band. Additionally, the decay times of the transients increase from <1 ps at 1954 cm^{-1} to 6 ps at 2034 cm^{-1}, matching the recovery time of the ground state band (6 ± 1 ps). The kinetic data are summarized in Table I.

MMCT excitation should lead to a complex in which the ruthenium cyanide center has formally changed from a 2+ to a

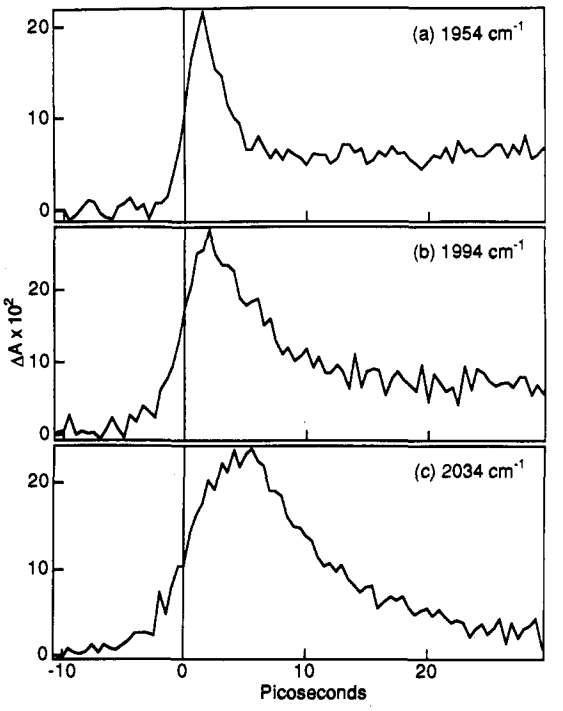

Figure 7. Transient decays obtained at (a) 1954, (b) 1994, and (c) 2034 cm^{-1} with 0.04 M Ru–Ru in D_2O following 600-nm excitation.

Table I. Rise and Decay Times in Ru–Ru for the Best Fit to Data from 1954 to 2060 cm^{-1} (600-nm Excitation)[a]

wavelength (cm^{-1})	rise time (ps)	fall time (ps)
1954	0.1	0.7
1974	0.3	1.9
1994	0.6	3.6
2014	0.7	4.6
2034	1.4	5.9
2060[b]	0.0	6.9

[a] Values given correspond to the best fit obtained when convolving the instrument response (typically a 3–4 ps fwhm $sech^2$ function) with a biexponential function; estimated relative error is ±0.5 ps. [b] Ground state bleach.

3+ oxidation state. Such a change in oxidation state is expected to shift the ground state frequency to ~2120 cm^{-1}.[19] Thus, we assign the band centered at 2110 cm^{-1} in the transient spectrum to the initially populated MMCT excited state. The features between 1950 and 2040 cm^{-1} are consistent with vibrationally hot ground state molecules formed upon return to the ground electronic state. Metal cyanide stretching vibrations exhibit anharmonicities of ca. 14 cm^{-1}, leading to vibrationally excited states that are shifted to lower energy from the ground state band.[20] The frequencies observed correspond to population of the v = 1–7 excited vibrational states.

When the MMCT excitation wavelength is changed from 600 to 700 nm, we again observe an instrument limited decrease in absorbance at the ground state IR frequency with a similar recovery time as found for 600-nm excitation. Due to interferences from coherence artifacts we were unable to conclusively observe the transient due to the MMCT excited state. We do observe production of vibrationally hot molecules of the ground electronic state. In the 700-nm case, however, we observe states up to only v = 5. Decay times for these transients were found to be similar

(19) We base this on comparison to model compounds, for example, $[(NC)_6Fe^{III}]^{3-}$ (2118 cm^{-1}) and $[(NC)_6Fe^{II}]^{4-}$ (2044 cm^{-1}); little difference is expected for the analogous ruthenium complexes. See: Nakamoto, K. *Infrared and Raman Spectra of Inorganic and Coordination Compounds*, 4th ed.; Wiley: New York, 1986; pp 272–273.

(20) Durand, D.; Scavarda do Carmo, L. C.; Lüty, F. *Phys. Rev. B* **1989**, *39*, 6096. This is also consistent with known MC≡O anharmonicities: Heilweil, E. J.; Cavanagh, R. R.; Stephenson, J. C. *Chem. Phys. Lett.* **1987**, *134*, 181 and references therein.

Table II. Rise and Decay Times in Ru–Ru for the Best Fit to Data from 1985 to 2035 cm^{-1} (700-nm Excitation)[a]

wavelength (cm^{-1})	rise time (ps)	fall time (ps)
1985	0.1	2.3
1995	0.1	3.2
2006	0.1	4.8
2016	0.9	5.5
2035	1.5	4.5
2061[b]	0.0	5.6

[a] Values given correspond to the best fit obtained when convolving the instrument response (typically a 3–4 ps fwhm $sech^2$ function) with a biexponential function; estimated relative error is ±0.5 ps. [b] Ground state bleach.

Table III. Rise and Decay Times in Os–Os for the Best Fit to Data from 1920 to 2050 cm^{-1} (600-nm Excitation)[a]

wavelength (cm^{-1})	rise time (ps)	fall time (ps)
1920	0.1	1.8
1940	0.1	3.8
1960	0.4	4.4
1980	0.9	6.0
2000	0.8	12.4
2016	1.0	18.0
2050[b]	0.0	19.0

[a] Values given correspond to the best fit obtained when convolving the instrument response (typically a 3–4 ps fwhm $sech^2$ function) with a biexponential function; estimated relative error is ±0.5 ps. [b] Ground state bleach.

to those produced with 600-nm excitation (see Table II), but the rise times were consistently faster (*vide infra*).

MMCT excitation at 600 nm leads to similar results in the Os–Os dimer. An instrument-limited decrease in the absorbance of the ground state band at 2040 cm^{-1} is observed. The recovery of this band, however, is a factor of 3 times slower than found for Ru–Ru, with $\tau = 19 \pm 1$ ps (see Figure 5b). A transient absorption band is also observed at lower energy from 1920 to 2020 cm^{-1}, corresponding to the hot vibrational states $v = 1$–7. As found for the Ru–Ru dimer, the rise and decay times for these states steadily increase as one moves from the low-energy to the high-energy side of the band. Rise times increase from an instrument-limited response (<0.5 ps) to 1.4 ps, while the decay times increase from 1.8 to 18 ps for decay of the $v = 1$ state, corresponding to the recovery time of the ground state absorbance. These kinetic results are summarized in Table III. Note that all decay times for the vibrationally hot species are slower than found for the corresponding vibrational states in the Ru–Ru dimer. In contrast, the rise times for both dimers are surprisingly quite similar. Attempts to observe the transient corresponding to the Os(III) cyanide stretch of the MMCT excited state were unsuccessful due to interferences from a small coherence artifact.[21] The coherence artifact also interfered somewhat with data collection across the hot band absorbance, but it is only a minor component of these transients.

Discussion

The general picture that emerges from our data is shown schematically in Figure 8. Visible excitation into the MMCT band produces, within the laser pulse, a charge transfer excited state that is well-described as a full charge transfer from the Ru–cyanide site to the Ru–ammine site. The charge transfer excited state decays within our time resolution ($\tau < 0.5$ ps) to produce vibrationally excited ground electronic state dimer. The limit we place on the back electron transfer rate is consistent with both theoretical estimates and experimental measurements of

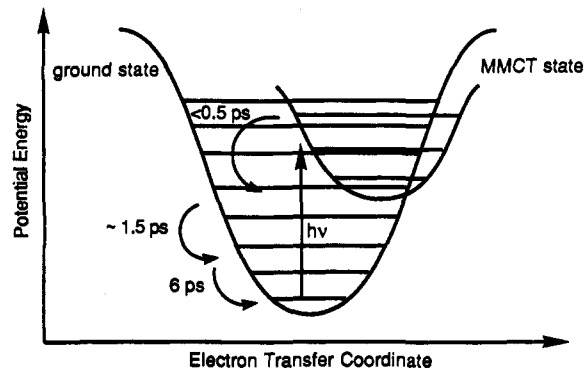

Figure 8. Simplified scheme for decay of excited state energy and vibrational relaxation processes.

the rate, which indicate a lifetime of ~100 fs for the charge transfer state.[11] Our observation of a RuC≡N stretching frequency consistent with ruthenium being in the 3+ oxidation state clearly demonstrates that a full charge transfer has occurred.

The instrument-limited rise times observed for the transient cyanide absorbances corresponding to high-lying v states ($v \approx 6$–7) show that return to the ground electronic state (i.e. back electron transfer) can result in production of highly vibrationally excited dimer, with the possibility of localization in the cyanide vibrations. The rise times of the lower-lying vibrational states get progressively slower, mirroring the increasing decay times for the higher vibrational states in Ru–Ru (Table I). This is consistent with the higher-lying states being precursors to the lower-lying states. The final step in Figure 8 illustrates relaxation of the $v = 1$ state to reproduce ground state dimer.

Inspection of the rise and fall times for the various vibrational states of the Ru–Ru dimer, and especially of the Os–Os dimer, however, indicates that the general scheme shown in Figure 8 is overly simplified. Specifically, if overlapping bands are neglected and we assume that vibrational cooling occurs via sequential one-quantum processes, we should observe rise times which are much slower. For example, the rise time for a frequency assigned to $v = 4$ should be equal to the decay time for $v = 5$; this is not observed. Additionally, while the rise times for the osmium derivative are comparable to those found for the ruthenium derivative, the decay times are ca. 3 times slower (see Tables I and III). Consideration of overlapping vibrational states and the possibility of multi-quantum cooling is unable to account for the large difference in the observed appearance and decay times. Instead the situation is clearly more complex, as expected for large molecules in the solution phase, in that a distribution of vibrational states is produced directly upon return to the ground electronic state. A more extensive analysis of the rates and mechanism for the vibrational relaxation which occurs after the back electron transfer will be presented in a future publication.[22] Here we will concentrate on the electron transfer aspects of the reaction.

Shown in Figure 9 (dotted line) is a plot of absorbance vs vibrational state at 1 ps for the ruthenium derivative generated from kinetic traces taken at selected wavelengths and corrected for the oscillator strength of a given transition.[23] While the presence of rise/decay times of the same magnitude as our pulsewidths complicates the interpretation, it is apparent that a distribution of vibrational states is present at 1 ps and is centered near $v = 1$–2. This suggests that low-lying vibrational states should show biexponential rises (an instantaneous and a slower

(21) Although coherence artifacts interfered with observation of the charge transfer excited state in Ru–Ru at 700-nm excitation and for Os–Os, we are confident that the transient we observed at 2110 cm^{-1} for Ru–Ru with 600-nm excitation is genuine. This transient absorption band was reproducible from day to day and displayed no coherence artifacts on either side of the band.

(22) Dyer, R. B.; Doorn, S. D.; Stoutland, P. O.; Woodruff, W. H. Manuscript in preparation.

(23) We have corrected for differing oscillator strengths using the harmonic oscillator assumption for which oscillator strength scales linearly with v state. Corrections have also been made to compensate for the fact that short-lived transients have reduced intensities compared to what they would have been had the species had a lifetime long compared to the instrument response.

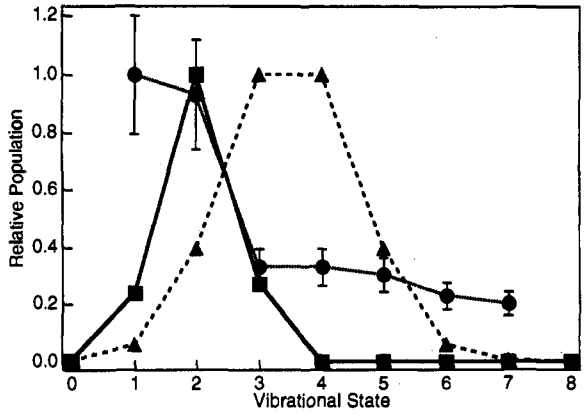

Figure 9. Relative population distributions for the range of observed v states in Ru–Ru following return to the ground electronic state: (···) experimental distribution; (- - -) calculated distribution using ν_q = 1191 cm^{-1}; (—) calculated distribution using ν_{q1} = 2109 cm^{-1} and ν_{q2} = 456 cm^{-1} (see text).

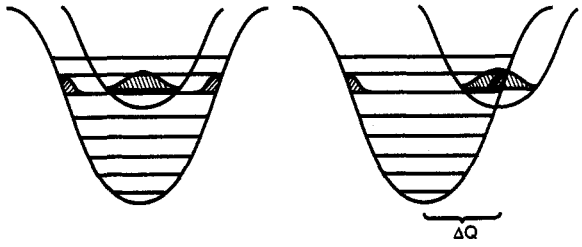

Figure 10. Simplified relationship between normal mode displacement (ΔQ) and Franck–Condon overlap between the ground and excited states.

component). Our time resolution does not allow us to resolve this. Our results represent, to the best of our knowledge, the first observations in the condensed phase of vibrational excitation coupled to an electron transfer reaction.[24]

Before proceeding with a detailed analysis of these results, some general comments are in order. Our experiments indicate that most of the ground state molecules are formed with relatively small amounts of excess energy in the MC≡N mode (1–3 quanta), but it is clear that in some cases ground state molecules are formed in which large amounts (up to 7 quanta) of energy are present in the MC≡N mode. This degree of excitation represents a remarkable localization of ~14 000 cm^{-1} of the available energy of 16 667 cm^{-1} in the case of a 600-nm photon.[25] The origin of this excitation is central to understanding the role of acceptor vibrations in ultrafast electron transfer reactions.

Upon back electron transfer the difference in energy between the two states (i.e. the 0 ← 0 transition energy) will be deposited into vibrational/rotational modes of the ground state. In general, the distribution of this energy will be among many modes, and it will be determined by how particular modes couple the two electronic states. In Figure 10 we illustrate two cases, one in which a particular mode is invariant in going from one electronic state to the next, and one in which there is a significant change, or displacement. Despite the simplicity of these one-dimensional drawings, they illustrate that ground state modes that are significantly displaced relative to those in the excited state provide for increased vibrational overlap (i.e. coupling) between low-lying vibrational states in the excited electronic state with high-lying vibrational isoenergetic states of the ground electronic state. This enhanced orbital overlap accelerates return to the ground state with concomitant excitation into these "accepting" modes. Resonance Raman experiments performed on the full range of the cyanide bridged dimers have demonstrated that both low-frequency metal–ligand vibrations associated with the ammine and cyanide sites of the dimers, and high-frequency vibrations of the terminal and bridging cyanides are significantly displaced during the charge transfer transition.[12a] Therefore, it is expected that both types of vibrations will be important energy acceptors. In general, however, for systems in which large amounts of energy are deposited into the ground electronic state, high-frequency modes serve as the best acceptors. This is a direct result of fewer quanta being required to accept a given amount of energy, which leads to increased vibrational overlap with high-frequency modes of the ground state.[26]

One puzzling aspect of these results is that we observe so much energy deposited into the infrared active MC≡N mode. This mode shows no resonance Raman intensity in the Ru–Ru dimer (although it does for Os–Os), suggesting that it should not be coupled to the charge transfer transition.[27] Our observation of excess energy in the infrared active mode of Ru–Ru suggests two possibilities. First, it is perhaps most likely that strong coupling between the Raman active and the infrared active cyanide modes leads to prompt appearance of vibrationally excited infrared active modes, independent of the mode initially populated upon return to the ground electronic state. Another possibility, however, is that the assumption that no resonance Raman intensity implies that a mode does not couple the ground and excited state surfaces is not valid. Such a situation might be envisioned in cases in which the ground and excited state surfaces are not well-described as harmonic oscillators having the same frequencies.

Our data should not be interpreted to imply that only this IR active mode acts as an acceptor vibration. The resonance Raman of these dimers shows that several low-frequency metal–ligand vibrations, as well as the bridging cyanide mode, are strongly coupled to the transition and should, therefore, serve as good acceptor vibrations.[12] In fact, prompt population of low-lying v states in the cyanide mode indicates that excess energy is available for deposition into these other active modes. The role of these other modes could, potentially, be addressed experimentally through ultrafast resonance Raman spectroscopy.

With these general concepts in mind, we have attempted to model the experimental results using quantum mechanical electron transfer theory developed by Jortner and Bixon.[4c] Related theoretical expressions have been developed, most recently by Barbara et al.,[28] providing a synthesis of the Jortner–Bixon and Sumi–Marcus[29] expressions by accounting for intramolecular vibrations with both a low-frequency classical mode and a high-frequency quantum mechanical mode. In applying these different models to the cyanide-bridged dimers, Barbara and co-workers have found that they yield similar results.[30] Thus, we have chosen the simpler Jortner–Bixon expressions to model the vibrational population distributions in the ground electronic state following the return electron transfer, since exclusion of the classical mode should not adversely affect the conclusions. The expression used

(24) Vibrationally excited products have been observed following electron transfer in the gas phase: (a) Liao, C. L.; Shao, J. D.; Xu, R.; Flesch, G. D.; Li, Y. G.; Ng, C. Y. *J. Chem. Phys.* **1986**, *85*, 3874, (b) Nieder, G.; Noll, M.; Toennies, J. P. *J. Chem. Phys.* **1987**, *87*, 2067 and references therein.

(25) A reviewer kindly pointed out that because return to the ground electronic state occurs within our pulse width, molecules might absorb a photon, return to the ground state surface, and absorb another photon. If this were happening it might lead to formation of very highly vibrationally excited ground state molecules. This is a possibility which we cannot completely discount. However, since we are exciting only ca. 10% of the molecules, qualitative arguments (assuming reasonable absorption cross sections for a hot ground state molecule, etc.) suggest that a negligible percentage of the molecules absorb more than one photon.

(26) Kober, E. M.; Caspar, J. V.; Lumpkin, R. S.; Meyer, T. J. *J. Phys. Chem.* **1986**, *90*, 3722 and ref 8f and references therein.

(27) Generally, only totally symmetric modes undergo displacement during an electron transfer. Thus, only these modes will be coupled to the electron transfer reaction or show resonance Raman intensity. Exceptions to this rule exist: the Jahn–Teller effect and 2-state Raman interference, for example. See: Tang, J.; Albrecht, A. C. In *Raman Spectroscopy, Theory and Practice*; Syzmanski, H. A., Ed.; Plenum: New York, 1970; Vol. 2, Chapter 2.

(28) Walker, G. C.; Åkesson, E.; Johnson, A. E.; Levinger, N. E.; Barbara, P. F. *J. Phys. Chem.* **1992**, *96*, 3728.

(29) Sumi, H.; Marcus, R. A. *J. Chem. Phys.* **1986**, *84*, 4894.

(30) Tominaga, D.; Kliner, D. A. V.; Johnson, A. E.; Levinger, N. E.; Barbara, P. F. *J. Chem. Phys.* Submitted for publication, and ref 12b.

for evaluating the electron transfer rate in Jortner–Bixon theory is shown in eq. 1:

$$k_{et} = \sum_{n=0} \frac{k_{NA}{}^{0n}}{1 + H_A{}^n} \quad (1)$$

This model views the total electron transfer rate (k_{et}) as the sum of individual rates ($k_{NA}{}^{0n}$) for relaxation into the different vibrational channels corresponding to the different v states (n) of a high-frequency quantum mechanical acceptor vibration. These nonadiabatic rates are scaled by an adiabaticity parameter ($H_A{}^n$) that includes the dependence of the rate on the solvent response time (τ_s). The relative populations present in each vibrational state following electron transfer are proportional to the relative rates into each vibrational channel. The terms $k_{NA}{}^{0n}$ and $H_A{}^n$ may be evaluated as follows:

$$k_{NA}{}^{0n} = \frac{2\pi V_n{}^2}{h\sqrt{4\pi\lambda_{solv}KT}} e^{-(\Delta E - nh\nu_q - \lambda_{solv})^2/4\lambda_{solv}kT} \quad (2)$$

$$H_A{}^n = \frac{4\pi V_n{}^2 \langle \tau_s \rangle}{h\lambda_{solv}} \quad (3)$$

In these expressions, ΔE is the electrochemical driving force for the reaction, λ_{solv} is the classically determined solvent reorganization energy, $nh\nu_q$ is the reorganization energy contribution from the appropriate excited vibrational state of the acceptor mode, $\langle \tau_s \rangle$ is the experimentally determined average solvation time, and V_n is the Franck–Condon "dressed" matrix element given by the product of the experimentally determined matrix element V and the nuclear Franck–Condon factor, $|\langle 0|n\rangle|$, given by eq 4:

$$|\langle 0|n\rangle| = \sqrt{\frac{S^n}{n!}e^{-S}} \quad (4)$$

where S is the Huang–Rhys factor $\Delta^2/2$, for which Δ is the unitless displacement of the normal coordinates of the acceptor vibration.

In order to simplify the calculations we have employed models with a reduced number of vibrational modes, specifically one and two vibrational modes. For the one-mode model an appropriate average value for the frequency (ν_q) of the acceptor vibration can be obtained from eq 5:

$$\nu_q = \sqrt{\sum_j \nu_j{}^2 \lambda_j / \lambda_{vib}} \quad (5)$$

where λ_{vib} is the total vibrational reorganization energy associated with the reaction and ν_j and λ_j are the individual mode frequencies and reorganization energy contributions to λ_{vib}. These parameters have been determined previously from an intensity analysis of the bands appearing in the resonance Raman spectrum of Ru–Ru.[31] For the two-mode problem we followed the procedure of Barbara et al.,[30] who grouped the eight Raman active modes into high- and low-frequency sets and then used eq 5. Except as noted, the other parameters used were obtained from the recently reported full band-shape analysis of the visible absorption band[30] and are listed in Table IV.

Using an average frequency (1191 cm^{-1}) calculated from eq 5 for Ru–Ru to determine the expected distribution of v states formed after electron transfer leads to the plot shown by the dashed line in Figure 9. It shows a maximum near the v = 3–4, with significant population in v states 2 and 5. Molecules with coupled high-frequency vibrations, however, might not be expected to be well-represented by an average frequency. Thus, we have also explored the use of two vibrational frequencies in an attempt to more accurately represent the problem. Using the procedure outlined above, we have performed the calculation using a high-frequency mode (2109 cm^{-1}) and a low-frequency mode (456 cm^{-1}) with appropriate reorganization parameters as listed in Table V.[32] Experimentally we observe a high-frequency mode, thus we have calculated the vibrational distribution in the high-frequency mode following electron transfer. This was done by calculating the rate into each vibrational state of the 2109-cm^{-1} mode for all vibrational states of the low-frequency (456 cm^{-1}) mode. The result, as shown by the solid line in Figure 9, is to shift the dominant acceptor channels to v = 1–3, in close agreement with the experimental results.

In order to estimate the uncertainty in these calculations, we have tried to make reasonable estimates as to the accuracy of any given parameter and the effect this would have on the calculation. Of the parameters used to calculate k^{0n}, varying V^2, $\langle \tau_s \rangle$, or S has very little effect on the vibrational distribution found (but can have an effect on the electron transfer rates). As expected, however, the calculation is sensitive to ΔE, λ_{solv}, and ν_q. Changing ΔE or λ_{solv} by 2000 cm^{-1}, for example, shifts the maximum of the vibrational state distribution by approximately one vibrational state. Similarly, for a one-mode simulation, changing ν_q from 1200 to 2000 cm^{-1} shifts the maximum of the vibrational distribution from v = 3–4 to 2.

We used values of ΔE and λ_{solv} calculated from the wavelength and shape of the visible absorption band. Alternatively ΔE can be estimated from electrochemical data of the individual metal complexes (i.e. each half of the dimer). From the similarities of ΔE calculated from the band shape and from the electrochemical data, we estimate that the value used is accurate to ±500 cm^{-1}. The value of λ_{solv} is somewhat more dependent on how it is calculated; we estimate it to be accurate to ±1500 cm^{-1}. Finally, while the calculation is sensitive to ν_q, it has been shown that the use of two modes accurately models the results found when all eight modes are used.[30] We thus assume that our values of ν_q are accurate enough to not adversely affect the results. On the basis of the estimates above, we believe that the maximum of the vibrational state distribution has an uncertainty of ±1 vibrational state.

Within this uncertainty, the calculations agree reasonably well with the experimental data except for our observation of prompt excitation in the higher vibrational states. The calculations predict that no significant population should be seen in the higher-lying v states. This discrepancy most likely arises from the assumption that the electron transfer reaction proceeds only from the v = 0

Table IV. Electron Transfer Parameters for Ru–Ru Used in the One-Mode Jortner–Bixon Calculation of Expected Vibrational Populations

parameter	value
V^2 [a]	3.6×10^6 (cm^{-1})^2
ΔE[b]	7880 cm^{-1}
λ_{solv}[b]	3700 cm^{-1}
(τ_S)[c]	0.59 ps
ν_q[d]	1191 cm^{-1}
S[e]	1.8
λ_{vib}[f]	2169 cm^{-1}

[a] Burewicz, A.; Haim, A. *Inorg. Chem.* **1988**, *27*, 1611. [b] Reference 30. [c] Reference 11a. [d] Calculated using eq 5 and frequency/reorganization data from ref 30. [e] S is also equivalent to λ_{vib}/ν_q. [f] Calculated from frequencies found in ref 12a and reorganization energies calculated in ref 30.

Table V. Electron Transfer Parameters for Ru–Ru Used in the Two Vibrational Mode Jortner–Bixon Calculation of Expected Vibrational Populations[a]

ν_i (cm^{-1})	$\lambda_{vib,i}$ (cm^{-1})	S
2109	619	0.29
456	1551	3.4

[a] Unlisted parameters are the same as those given in Table IV.

(31) We used ν_j as measured in the resonance Raman spectrum of ref 12, but we used the more recent values of λ_j calculated in ref 30.

(32) The frequencies and reorganization values were obtained by averaging the highest two frequencies (reorganization parameters) and the lowest six frequencies (reorganization parameters) obtained from the Raman spectra.

state of the excited state surface. Production of $v = 7$ vibrational excitation in the ground state (with 14 000 cm^{-1} of energy content) from $v = 0$ of the excited state (around 8000 cm^{-1} potential energy content[11]) clearly violates energy conservation. With excitation at 600 nm (16 667 cm^{-1}, ~8000 cm^{-1} higher than the $0 \leftarrow 0$ transition energy in Ru–Ru), however, it is possible to form higher vibrational states of the electronically excited state. Given the longer vibrational relaxation times as compared to that for the electron transfer reaction, it is expected that the reaction will proceed from a number of different vibrational states of the excited state surface. This effectively adds channels to the reaction that will populate higher-lying v states of the ground state surface.[4c] The relatively small displacements of the normal coordinates in the electronic excited state (determined from Raman spectroscopy), however, suggest that the initial population in the MC≡N mode prepared by the laser pulse will most likely be in states no higher than $v = 2$.[33] Calculations for the Os–Os dimer are similar except that the larger driving force for the reaction shifts the distribution to slightly higher vibrational states.

Our results using 700-nm excitation support this analysis. Excitation at this wavelength provides 2380 cm^{-1} less energy than at 600 nm and should result in less excitation in the electronic excited state. Our observations show that this is reflected in the ground state after electron transfer, with the distribution of excited v states being shifted to lower energies (v = 1–5). The kinetics associated with the vibrational excitation using the 700-nm pump pulse are in accord with this interpretation in that the rates of appearance of hot vibrational states v = 4–5 were consistently faster than seen with 600-nm excitation, implying that these states are being produced directly upon back electron transfer and not from cooling of higher-lying vibrational states.

Conclusions

Our studies of the vibrational dynamics coupled to the ultrafast electron transfer reactions in the cyanide-bridged dimers have provided additional insight into the nature and role of the important acceptor vibrations linked to the back electron transfer processes in these reactions. We have found that recent theoretical expressions for ultrafast electron transfer are successful in predicting excited vibrational populations resulting from back electron transfer in the Marcus "inverted region". The rates of vibrational relaxation in comparison to the electron transfer rate have potentially important consequences for ultrafast electron transfer reactions in general. Electron transfer theory generally assumes that reactions proceed out of a thermally equilibrated excited state. Our measured vibrational relaxation times (on the order of several picoseconds), however, are much slower than the electron transfer (~100 fs) in these dimers.[34] Thus, at least for certain systems, the assumption of thermal equilibrium in the excited state may not be a correct one. Barbara and co-workers[35] have shown that such a condition will not have a significant effect for inverted region electron transfer, but the same may not be true for ultrafast "normal region" electron transfer reactions. For such reactions, on the time scale of the charge transfer, the vibrations coupled to the reaction will remain activated and effectively decrease the vibrational reorganization barrier for the back electron transfer. Under such conditions electron transfer rates may be faster than predicted by theory. Such rate accelerations may prove to be of importance in such biological processes as the charge separation steps in photosynthesis.[36]

Acknowledgement. Support for this work by LANL Laboratory Directed Research Grants X15D and X15B is gratefully acknowledged. We thank Professor Paul F. Barbara for helpful discussions and disclosure of work prior to publication. This work was performed at Los Alamos National Laboratory under the auspices of the U. S. Department of Energy.

(33) This would suggest that we should still not see states higher than $v \sim 6$ upon return to the ground electronic state. While it is unclear how higher vibrational states are formed, it may be that ground state/excited state coupling leads to energy being transferred from other modes into the MC≡N mode during the back electron transfer. We do not expect this to be a favored process, but it may be sufficient to generate the relatively small amount of highly vibrationally excited states that we observe.

(34) We have measured vibrational relaxation rates in the ground electronic state. We are making the assumption that relaxation in the electronically excited state is not significantly different.

(35) Barbara, P. F. Personal communication.

(36) Recently it has been observed that charge transfer does indeed occur from a state that is not thermally equilibrated. Vos, M. H.; Lambry, J.-C.; Robles, S. J.; Youvan, D. C.; Breton, J.; Martin, J.-L. *Proc. Natl. Acad. Sci. U.S.A.* **1991**, *88*, 8885.